Advances in Remote Sensing, 2014, 3, 208-218
Published Online September 2014 in SciRes. http://www.scirp.org/journal/ars
http://dx.doi.org/10.4236/ars.2014.33014

Scientific Research

A Study on Tropical Land Cover Classification Using ALOS PALSAR 50 m Ortho-Rectified Mosaic Data

Lan Mi[1], Nguyen Thanh Hoan[2], Ryutaro Tateishi[1], Kotaro Iizuka[1], Bayan Alsaaideh[1], Toshiyuki Kobayashi[1]

[1]Center for Environmental Remote Sensing, Chiba University, Chiba, Japan
[2]Institute of Geography Vietnam Academy of Science and Technology (VAST), Hanoi, Vietnam
Email: miran@graduate.chiba-u.jp

Received 25 July 2014; revised 20 August 2014; accepted 16 September 2014

Abstract

The main objective of this study is to find better classifier of mapping tropical land covers using Synthetic Aperture Radar (SAR) imagery. The data used are Advanced Land Observing Satellite (ALOS) Phased Array type L-band Synthetic Aperture Radar (PALSAR) 50 m ortho-rectified mosaic data. Training data for forest, herbaceous, agriculture, urban and water body in the test area located in Kalimantan were collected. To achieve more accurate classification, a modified slope correction formula was created to calibrate the intensity distortions of SAR data. The accuracy of two classifiers called Sequential Minimal Optimization (SMO) and Random Forest (RF) were applied and compared in this study. We focused on object-based approach due to its capability of providing both spatial and spectral information. Optimal combination of features was selected from 32 sets of features based on layer value, texture and geometry. The overall accuracy of land cover classification using RF classifier and SMO classifier was 46.8% and 55.6% respectively, and that of forest and non-forest classification was 74.4% and 79.4% respectively. This indicates that RF classifier has better performance than SMO classifier.

Keywords

Slope Correction, Land Cover Classification, Feature Selection, Sequential Minimal Optimization, Random Forest

1. Introduction

Remote sensing techniques have been used for land cover mapping for several decades. Since the Synthetic

How to cite this paper: Mi, L., Hoan, N.T., Tateishi, R., Iizuka, K., Alsaaideh, B. and Kobayashi, T. (2014) A Study on Tropical Land Cover Classification Using ALOS PALSAR 50 m Ortho-Rectified Mosaic Data. *Advances in Remote Sensing*, **3**, 208-218.
http://dx.doi.org/10.4236/ars.2014.33014

Aperture Radar (SAR) has been applied to monitor land cover distribution, the Earth's surface information can be observed in high resolution regardless of any weather condition [1]. SAR is a form of radar that has different penetration and different wavelength. Therefore, it performs subtle function on observing different land target. Generally, longer wavelength L-band SAR is tending to be more helpful for forest distribution monitoring [2] [3]. However, terrain influences caused by the side-looking technique of radar sensor had revealed significant brightness variations in SAR imagery. For example, the foreside of a slope area is always more illuminated than the backside in terms of a smaller incidence angle, even though the radar reflectivity is from homogeneous scattering type [4] [5].

In January 2006, Japan Aerospace Exploration Agency (JAXA) successfully launched the Advanced Land Observing Satellite (ALOS). The Phased Array type L-band Synthetic Aperture Radar (PALSAR) is one of three onboard remote-sensing instruments, which is used for day-and-night and all-weather land observation [6]. The ALOS Kyoto and Carbon (K & C) Initiative, an international collaborative project led by the Earth Observation Research Center (EORC) of JAXA created ALOS PALSAR 50 m ortho-rectified mosaic dataset with the fine-beam dual polarization (FBD) mode to provide HH and HV channels covering Japan, Kalimantan, Central Africa and other eight large areas [7]. As a free product, many studies have shown its high potential for land cover observation and classification because the geometric correction and geographic coordinate have been processed [8]-[10]. However, some studies only chose the flat terrain as study areas due to slope correction has not yet been done for keeping the landscape characteristics [11] [12].

In order to extract high accuracy land cover information, the normalized SAR imagery is required for classification quality. In addition to using backscatter coefficient as radar measure, the gamma-naught (γ°) which can be calculated with $\sigma^{\circ}/\cos\theta_{loc}$ shows a stronger capability for forest data analysis, where σ° and θ_{loc} mean the normalized cross section and local incidence angle, respectively. However, there is still limitation of terrain height within this equation [1] [3] [13]. Furthermore, other calibration methodologies, like the correction based on the covariance matrix and the ground scattering area variation, were frequently applied the terrain correction before geocoding that represent better effect [14] [15]. Thus, the order of data processing would affect the calibration effect of SAR image.

On the other hand, for high resolution remote sensing imagery classification, image segmentation may provide lots of object information not only about spectral, but also about the spatial or shape features. With the using of object-based approaches, some scientific literatures have shown the improved classification accuracy when compared with traditional pixel-based techniques [16] [17]. Therefore, object-based approach was chosen to be used in this study.

The objectives of this paper are: 1) to remove the terrain influence on HH and HV polarization of ALOS PALSAR 50 m ortho-rectified mosaic data; 2) to identify the better classification performance between Sequential Minimal Optimization (SMO) classifier and Random Forest (RF) classifier.

2. Study Area and Satellite Data

2.1. Study Area

In order to investigate the possibility of land cover classification by using ALOS PALSAR 50m ortho-rectified mosaic data, the proposed approach was tested on a tropical zoon where covered by tropical forest, herbaceous, agriculture, urban and water body. This testing area is located within the West Coast Division of Sabah, Malaysia (116d01'55.7685"E, 5d56'25.2183"N and 116d08'43.2737"E, 5d51'19.5894"N), approximately 12.53 km × 9.39 km. The DEM (Digital Elevation Model) ranges from 0m to 507 m. **Figure 1** shows the location of study area with the color composite image of PALSAR data (R = HH, G = HV, B = HH − HV).

2.2. Satellite Data and Image Preprocessing

The ALOS PALSAR 50 m ortho-rectified mosaic data and Shuttle Radar Topography Mission (SRTM) are the main satellite data used in this study. These datasets are available at the K & C mosaic homepage and the Consultative Group on International Agricultural Research-Consortium for Spatial Information (CGIAR-CSI) website.

PALSAR 50 m ortho-rectified mosaic data are obtained from July to October, 2008, which include HH polarization and HV polarization. We resampled 90 m SRTM data to a pixel size of 50 m × 50 m using the bilinear

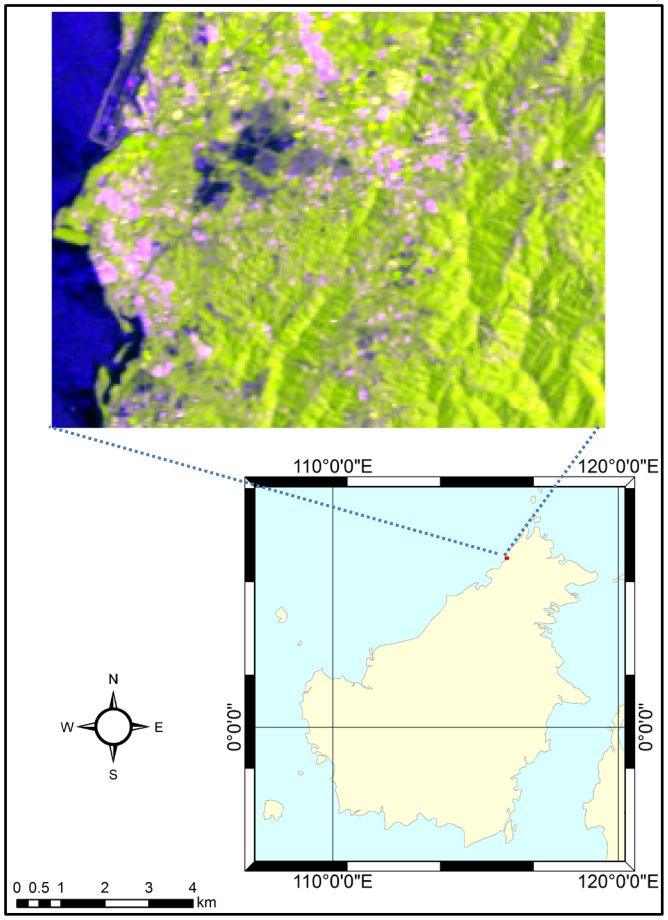

Figure 1. Composite RGB image of PALSAR data over study area. (R: HH; G: HV; B: HH − HV).

interpolation in order to correspond with HH and HV images. Then, Landsat images were chosen as standard to correct geometric location of PALSAR mosaic images and SRTM by using Ground Control Points (GCPs).

Digital Number (DN) of HH and HV polarization images were converted to the normalized radar cross section (Sigma-zero) by the following equation [18]:

$$\sigma^{\circ} = 10 \times \log_{10} DN^2 + CF \tag{1}$$

where *DN* is the digital number of HH and HV images, Calibration Factor (*CF*) for ALOS PALSAR 50 m ortho-rectified mosaic had been given as (−83) and σ° is the backscattering coefficient (dB).

3. Slope Correction

3.1. Previous Slope Correction Models

Some methods of calibration need to be applied to original SAR data before further investigation, because of the amount of distortion that happens on the image (e.g., Speckle filtering, geometric correction and radiometric correction). As an important processing step to reduce the topography influence, different slope correction models had been generated based on the cosine correction method and the scattering area changing method. Many of these models were dealt with the terrain correction with different code-level programming or software tool [19] [20]. Therefore, the order of data processing or the processing environment may result in different slope correction effect. In this section, three existing slope correction models were tested to perform their restoration capability for ALOS PALSAR 50m ortho-rectified mosaic data. The brief description of these models is shown in **Table 1**.

Table 1. Three existing slope correction models.

	Existing slope correction models		
	Model_1	Model_2	Model_3
Equation expression	$R_c = \frac{R}{\cos^4\theta_{loc} + (1-\cos^4\theta_{loc})}$	$\sigma^o_{corr} = \sigma^o \frac{\sin\theta_{loc}}{\sin\theta_{ref}}$	$\gamma^o = \sigma^o \frac{A_{flat}}{A_{slope}} \left(\frac{\cos\theta_{ref}}{\cos\theta_{loc}}\right)^n$
Authors	Akatsuka *et al.* (2009); Japan Aerospace Exploration Agency (2009)	Kellndorfer *et al.* (1998); Rokhmatuloh *et al.* (2012)	T. Castel *et al.* (2001); M. Santoro (2011)
Symbol explanation	R_c: Corrected digital number of SAR image R: Original digital number of SAR image θ_{loc}: Local incidence angle	σ^o_{corr}: SAR backscatter coefficient after calibration σ^o: Original SAR backscatter coefficient θ_{loc}: Local incidence angle θ_{ref}: SAR incidence angle at the center of the image	γ^o: SAR backscatter coefficient after calibration σ^o: Original SAR backscatter coefficient A: Local ground scattering area within a pixel θ_{loc}: Local incidence angle θ_{ref}: Incidence angle at mid-swath n: $0.7 \le n \le 1$

Model-1 and model-2 were proposed by the cosine correction method [21]-[24], while model-3 was proposed based on the scattering changing method [25] [26]. The main calculation steps consist of:

1) Calculation of local incidence angle (θ_{loc})

In this study, θ_{loc} was derived by the following equation which described by Akatsuka *et al.* [21]:

$$\cos\theta_{loc} = \cos\theta\cos\alpha + \sin\theta\sin\alpha\cos(\varnothing - \beta) \tag{2}$$

Here, the slope α and aspect angle β of SRTM were exported from spatial analyst tools of ArcGIS software. The azimuth angle of PALSAR platform $\varnothing$ is 261.84 degree, and θ is equal with the off-nadir angle 34.3 degree.

2) Calculation of local ground scattering area (A)

Castel *et al.* [25] provided a sample equation to describe A over a flat terrain as the following equation:

$$A_{flat} = \frac{r_a r_s}{\sin\theta_{loc}} \tag{3}$$

where r_a and r_s represent the azimuth and slant range pixel spacing respectively. On the other hand, the method for computing A_{slope} was selected from the literature published by Wegmuller [27]:

$$A_{slope} = \frac{r_a r_s}{\cos\psi} \tag{4}$$

where ψ is the projection angle which defined as the angle between the surface normal and the image plane normal [28]:

$$\cos\psi = \sin\theta\cos\alpha + \cos\theta\sin\alpha\sin\beta \tag{5}$$

Here, α, β and θ represent the same meaning within Equation (2).

3) Value decision of θ_{ref} and n

θ_{ref} of model-2 and model-3 means a reference incidence angle which was defined as 34.3 degree in this study. Model-3 was applied to correct ALOS PALSAR 50m ortho-rectified mosaic HH and HV image when n is 0.7.

3.2. A modified Slope Correction Model

Based on a sample backscatter terrain correction model, a modified slope correction model for specially calibrating ALOS PALSAR 50 m ortho-rectified mosaic data of this study was generated with the regulation that the homogeneous land cover target should have the similar backscattering property regardless of any topography terrain [23]. This sample model had been published by Ulaby *et al.* [29] and Sun *et al.* [30] as:

$$\sigma^\circ = \sigma\cos^p\theta_{loc} \tag{6}$$

where σ and σ° are backscattering coefficient before and after terrain correction, respectively. Sun *et al.* [30] carried out this model both for HH polarization and HV polarization of L-band wave, and successfully induced the terrain effect with the changing of power *p*, where $1 \le p \le 2$. **Figure 2** and **Figure 3** show the corrected images of ALOS PALSAR 50 m mosaic data by using Equation (6) when *p* is 1. Slope corrected HV image (**Figure 2(b)**) shows a more efficient correction on brightness variation than HH image (**Figure 3(b)**) over the mountain areas. Therefore, the limitation of this model is required to be improved for HH image.

Figure 4 shows a sample scattering geometry on the ground surface. Suppose the scattering surface over flat area that has standard backscattering behavior, each target over the tilted area will get an assumptive standard reference. Therefore, in **Figure 4**, A is a real target point (one pixel) of inclined plane face with satellite, the backscattering coefficient of B (σ_B) is considered as A (σ_A)'s standard behavior. Local incidence angle of B is equal to the off-nadir angle (incidence angle at the center of the image, θ_{ref}). Then, we can derive the relationship of A and B with backscattering coefficient and local incidence angle as Equation (7):

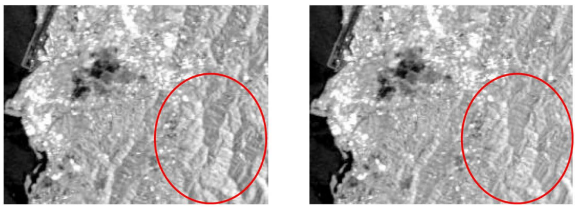

(a) (b)

Figure 2. Slope corrected result of HH image by using Equation (6). (a): Original HH image; (b): Slope corrected HH image.

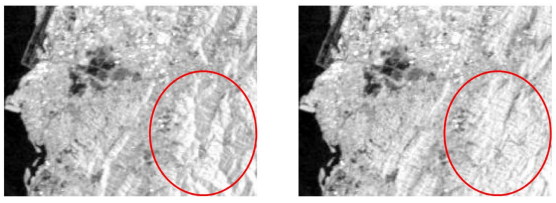

(a) (b)

Figure 3. Slope corrected result of HV image by using Equation (6). (a): Original HV image; (b): Slope corrected HV image.

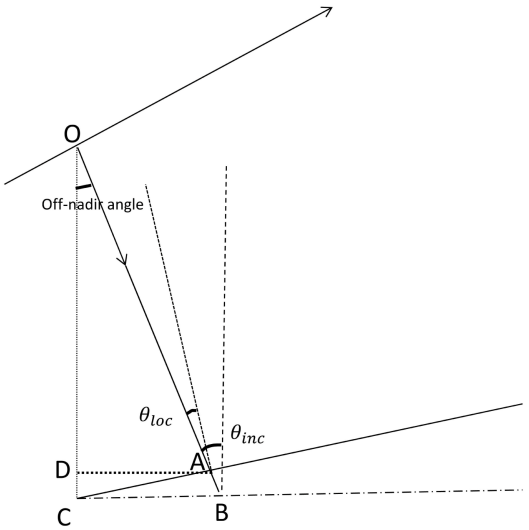

Figure 4. Ground scattering geometry. θ_{loc} is the local incidence angle, θ_{inc} is 34.3 degree.

$$\sigma_B \cos\theta_{ref} = \sigma_A \cos\theta_{loc} \tag{7}$$

Therefore, the assumptive standard backscattering behavior (σ_B) can be calculated from Equation (7):

$$\sigma_B = \sigma_A \frac{\cos\theta_{loc}}{\cos\theta_{ref}} \tag{8}$$

Here, we call $\left(\cos\theta_{loc}/\cos\theta_{ref}\right)$ as the strengthened correction factor for HH polarization. In addition, according to the geometry theorem, the power of p is decided by the relationship of OB and OA:

$$\frac{OB}{OA} = \frac{OC}{OD} = \frac{H}{H-h} \tag{9}$$

where H is the satellite's height, and h is the DEM. Combing the equations above, leads to the new terrain correction model for ALOS PALSAR 50 m mosaic data following with:

$$\sigma^{o}_{corr\_HH} = \sigma^{o}_{HH} \cos^{\frac{H}{H-h}}\theta_{loc} \frac{\cos\theta_{loc}}{\cos\theta_{ref}} \tag{10}$$

$$\sigma^{o}_{corr\_HV} = \sigma^{o}_{HV} \cos^{\frac{H}{H-h}}\theta_{loc} \tag{11}$$

where $\sigma^{o}_{corr\_HH}$ and $\sigma^{o}_{corr\_HV}$ mean the backscatter coefficient after slope correction for HH image and HV image, and σ^{o}_{HH} and σ^{o}_{HV} mean the original backscatter coefficient of HH image and HV image, respectively.

The effect of each slope correction model is assessed by visual identification in **Figure 5** and **Figure 6**. As can be seen, model-1, model-2 and model-3 have less impact on changing the backscattering brightness variation over mountain area, while the corrected image generated using Equation (10) and Equation (11) show the mountain area had been changed to flat.

4. Classification

4.1. Feature Selection

Based on the slope corrected images, firstly, a multi-layer image was composited using four layers that are HH, HV, the difference between HH and HV (HH-HV) and the ratio of HH and HV (HH/HV). Image segmentation was derived from a commercial software tool, eCognition 9.0. Multiresolution segmentation method was applied

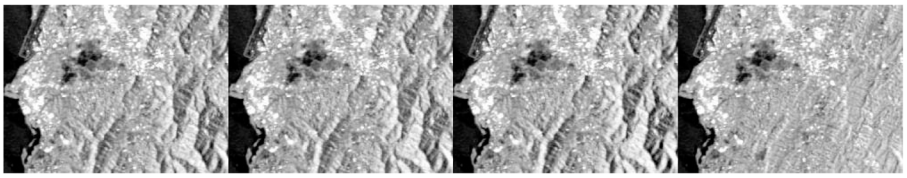

(a) (b) (c) (d)

Figure 5. Slope correction results of HH image extracted from each slope correction model. (a): Corrected by model-1; (b): Corrected by model-2; (c) Corrected by model-3; (d) Corrected by Equation (10).

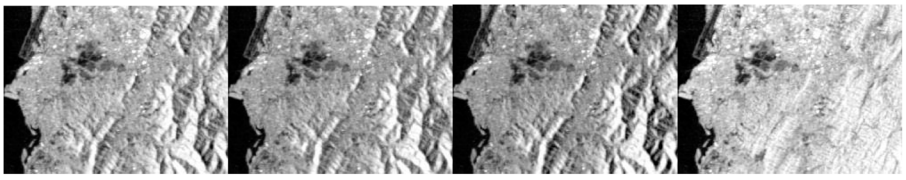

(a) (b) (c) (d)

Figure 6. Slope correction results of HV image extracted from each slope correction model. (a): Corrected by model-1; (b): Corrected by model-2; (c) Corrected by model-3; (d) Corrected by Equation (11).

to the composited image together with the ground truth training samples, which consist of forest, herbaceous, agriculture, urban and water body. 2552 objects were generated along with the scale decided as 2. We extracted 32 object features based on the layer value, texture and geometry properties for HH, HV, HH-HV and HH/HV individually (**Table 2**).

In order to reduce the useless features to improve the accuracy for the subsequent classifiers Sequential Minimal Optimization (SMO) and Random Forest (RF), we chose to use Weka software tool, which is used for a correction of fast machine learning algorithms of data mining, to find an optimal feature combination and classification. The feature selection result extracted from Wrapper Subset Evaluation is shown in **Table 3**.

4.2. Classification and Validation Results

The predicted land cover classification results exported from Weka software tool are shown in **Figure 7(a)** and **Figure 7(b)**. Images available in Google Earth were used as ground truth to evaluate the accuracy of SMO and RF classifier. 50 points were randomly collected for each class from the classification result. Due to the classification result of SMO that did not show any agriculture class, we collected 50 validation random points from agriculture ground truth to identify which class did they misclassified into. **Table 4(a)** and **Table 5(a)** show the result of accuracy assessment of five land cover classes classified by SMO classifier and RF classifier. The overall accuracy and kappa coefficient were 46.8% and 0.335 for SMO classification result, while 55.6% and 0.445 for RF classification result. From **Table 4(a)**, 28 validation points of agriculture were misclassified as forest, 13 points were misclassified to herbaceous and 9 points were misclassified as urban. The validation result identified with random points of the water body is 100% for both SMO and RF, while one segmented object was obviously misclassified as agriculture over the ocean in **Figure 7(b)**. In order to solve this problem, we considered to alter this misclassified segment by hand in this case, while to make water body mask using the different satellite image or replace water body class with the result from RF classifier when classify larger study area.

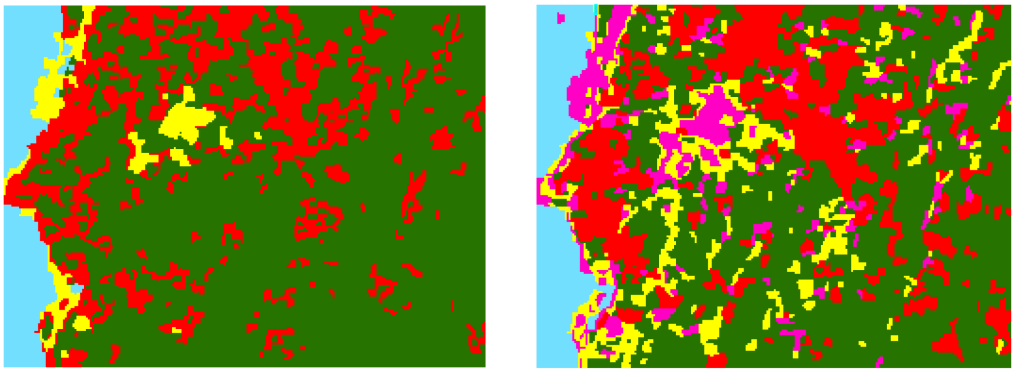

(a) (b)

Figure 7. Classification results predicted by Weka software tool.(a): SMO classifier; (b): RF classifier. Green: forest**;** Yellow: herbaceous; Pink: agriculture; Red: urban; Blue: water body.

Table 2. The list of generated features from eCognition Developer.

Layer value feature	Texture feature	Geometry feature
(1) Mean (2) Mode (3) Quantile (4) Standard Deviation (5) Skewness (6) Border Contrast (7) Circular Mean (8) Circular StdDev (9) CircularStdDev/Mean	(10) GLCM Homogeneity (11) GLCM Contrast (12) GLCM Dissimilarity (13) GLCM Entropy (14) GLCM Ang.2nd moment (15) GLCM Mean (16) GLCM StdDev (17) GLCM Correlation (18) GLDV Ang.2nd moment (19) GLDV Entropy (20) GLDV Mean (21) GLDN Contrast	(22) Asymmetry (23) Border index (24) Compactness (25) Density (26) Elliptic Fit (27) Main direction (28) Radius of Largest Enclosed ellipse (29) Radius of Smallest enclosing ellipse (30) Rectangular Fit (31) Roundness (32) Shape index

Table 3. Optimal feature combination for SMO and RF.

Classifier	Optimal feature combination
SMO	Quantile_HV Standard Deviation_HV Skewness_HV Skewness_(HH-HV) Border Contrast_(HH/HV) Circular Mean_HV Circular StdDev/Mean_HV Circular StdDev/Mean_(HH-HV)
RF	Mean_HH Circular Mean_HH Circular StdDev/Mean_(HH-HV) Elliptic Fit

Table 4. (a) Accuracy of land cover classification result of SMO classifier; (b) Accuracy of forest and non-forest result of SMO classifier.

(a)

Classification	Forest	Herbaceous	Agriculture	Urban	Water	Total	User's accuracy
Forest	**29**	1	28	14	0	72	40.3%
Herbaceous	10	**13**	13	10	0	46	28.3%
Agriculture	1	16	**0**	0	0	17	0
Urban	10	1	9	**25**	0	45	55.6%
Water	0	19	0	1	**50**	70	71.4%
Total	50	50	50	50	50	**250**	
Producer's accuracy	58%	26%	0	50%	100%		
Overall accuracy				46.8%			
Kappa coefficient				0.335			

(b)

Classification	Forest	Non-forest	Total	User's accuracy
Forest	**29**	43	66	43.9%
Non-forest	21	**153**	184	83.2%
Total	50	200	**250**	
Producer's accuracy	58%	76.5%		
Overall accuracy			74.4%	
Kappa coefficient			0.286	

Table 5. (a) Accuracy of land cover classification result of RF classifier; (b) Accuracy of forest and non-forest result of RF classifier.

(a)

Classification	Forest	Herbaceous	Agriculture	Urban	Water	Total	User's accuracy
Forest	**32**	10	6	18	0	66	48.5%
Herbaceous	7	**25**	18	8	0	58	43.1%
Agriculture	2	3	**8**	0	0	13	61.5%
Urban	9	11	12	**24**	0	56	42.9%
Water	0	1	6	0	**50**	57	87.7%
Total	50	50	50	50	50	**250**	
Producer's accuracy	64%	50%	16%	48%	100%		
Overall accuracy				55.6%			
Kappa coefficient				0.445			

(b)

Classification	Forest	Non-forest	Total	User's accuracy
Forest	**32**	34	66	48.5%
Non-forest	18	**166**	184	90.2%
Total	50	200	**250**	
Producer's accuracy	64%	83%		
Overall accuracy			79.4%	
Kappa coefficient			0.42	

Forest and non-forest classification accuracy was also assessed using the same random validation points (**Table 4(b)** and **Table 5(b)**). RF classifier showed a better performance with overall accuracy of 79.4% and kappa coefficient of 0.42, while the overall accuracy of SMO was 74.4% and kappa coefficient was 0.286.

5. Conclusions

Slope correction and object-based classification approach have been described in this study. In terms of slope correction, the visual inspection of the corrected images demonstrated the new modified slope correction model that has the ability of reducing the terrain influence on ALOS PALSAR 50m ortho-rectified mosaic HH polarization as well as HV polarization. The reason of unavailable of the exiting slope models are considered as that may be caused by using different software tool (model-1), different code-level programming (model-2) and the determination of parameter (model-3).

In terms of classification, Sequential Minimal Optimization (SMO) was compared with Random Forest (RF) classifier after feature selection. Eight features were selected for SMO, while four features were selected for RF automatically by Weka software tool. The accuracy assessment represented that the use of RF is better than SMO for multiclass land cover classification with a higher overall accuracy and kappa coefficient. In order to avoid the overfitting problem occurred on the result of SMO, adding more ground truth data is considered in the future. Then, we will test SMO and RF classifiers on different location and larger area multiclass land cover classification.

Acknowledgements

The authors would like to appreciate Japan Aerospace Exploration Agency (JAXA) Earth Observation Research Center (EORC) for providing the free ALOS PALSAR 50 m ortho-rectified mosaic product to support kinds of remote sensing researches.

References

[1] Shimada, M. (2010) Ortho-Rectification and Slope Correction of SAR Data Using DEM-based Simulated Data and Its Accuracy Evaluation. *IEEE Journal of Selected Topics in Applied Earth Observations and Remote Sensing*, **3**, 657-671. http://dx.doi.org/10.1109/JSTARS.2010.2072984

[2] Shimada, M. and Ohtaki, T. (2010) Generating Large-Scale High-Quality SAR Mosaic Datasets: Application to PALSAR Data for Global Monitoring. *IEEE Journal of Selected Topics in Applied Earth Observations and Remote Sensing*, **3**, 637-656. http://dx.doi.org/10.1109/JSTARS.2010.2077619

[3] Anthony, F. (1992) SAR Calibration: An Overview. *IEEE Transactions on Geoscience and Remote Sensing*, **30**, 1107-1121. http://dx.doi.org/10.1109/36.193786

[4] Bayer, T., Winter, R. and Schreier, G. (1991) Terrain Influences in SAR Backscatter and Attempts to their Correction. *IEEE Transactions on Geoscience and Remote Sensing*, **29**, 451-462. http://dx.doi.org/10.1109/36.79436

[5] Sun, N. and Ranson, K.J. (2001) Terrain Effect on Forest Radar Backscatter: Modeling and Correction. Committee on Earth Observation Satellites (CEOS) SAR Workshop, CEOS-SAR01-074.

[6] JAXA K & C Mosaic Homepage. http://www.eorc.jaxa.jp/ALOS/en/kc_mosaic/kc_mosaic.htm

[7] Rosenqvist, A., Ogawa, T., Shimada, M. and Igarashi, T. (2001) Initiating the ALOS Kyoto & Carbon Initiative. Insti-

tute of Electrical and Electronics Engineers (IEEE).
http://www.eorc.jaxa.jp/ALOS/kyoto/ref/IGARSS01_Rosenqvist-etal.pdf

[8] Jukka, M. and Soo, C.L.(2011)Separability of Insular Southeast Asian Woody Plantation Species in the 50 m Resolution ALOS PALSAR Mosaic Product. *Remote Sensing Letters*, **2**, 299-307. http://dx.doi.org/10.1080/01431161.2010.520345

[9] Dong, J., Xiao, X., Sheldon, S., Biradar, C., Duong, N.D. and Hazarika, M. (2012) A Comparison of Forest Cover Maps in Mainland Southeast Asia from Multiple Sources: PALSAR, MERIS, MODIS and FRA. *Remote Sensing of Environment*, **127**, 60-73. http://dx.doi.org/10.1016/j.rse.2012.08.022

[10] De Grandi, G.D., Bouvet, A., Lucas, R.M., Shimada, M., Monaco, S. and Rosenqvist, A. (2011) The K & C PALSAR Mosaic of the African Continent: Processing Issues and First Thematic Results. *IEEE Transactions on Geoscience and Remote Sensing*, **49**, 3593-3610. http://dx.doi.org/10.1109/TGRS.2011.2165288

[11] Shimada, M., Isoguchi, O. and Rosenqvist, A. (2008) Continent Scale PALSAR Mosaic Products for Kyoto and Carbon Project, Institute of Electronics. Information and Communication Engineers, 81-86.

[12] Longepe, N., Rakwatin, P., Isoguchi, O., Shimada, M., Uryu, Y. and Yulianto, K. (2011) Assessment of ALOS PALSAR 50 m Orthorectified FBD Data for Regional Land Cover Classification by Support Vector Machines. *IEEE Transactions on Geoscience and Remote Sensing*, **49**, 2135-2150. http://dx.doi.org/10.1109/TGRS.2010.2102041

[13] David, S. (2011) Flattening Gamma: Radiometric Terrain Correction for SAR Imagery. *IEEE Transactions on Geoscience and Remote Sensing*, **49**, 3081-3093. http://dx.doi.org/10.1109/TGRS.2011.2120616

[14] Chen, S.W., Wang, X.S. and Sato, M. (2012) PolInSAR Complex Coherence Estimation Based on Covariance Matrix Similarity Test. *IEEE Transactions on Geoscience and Remote Sensing*, **50**, 4699-4710. http://dx.doi.org/10.1109/TGRS.2012.2192937

[15] Luckman, A.J. (1998) Correction of SAR Imagery for Variation in Pixel Scattering Area Caused by Topography. *IEEE Transactions on Geoscience and Remote Sensing*, **36**, 344-350. http://dx.doi.org/10.1109/36.655350

[16] Hussain, M., Chen, D., Cheng, A., Wei, H. and Stanley, D. (2013) Change Detection from Remotely Sensed Images: From Pixel-Based to Object-Based Approaches. *ISPRS Journal of Photogrammetry and Remote Sensing*, **80**, 91-106. http://dx.doi.org/10.1016/j.isprsjprs.2013.03.006

[17] Blaschke, T. (2010) Object Based Images Analysis for Remote Sensing. *ISPRS Journal of Photogrammetry and Remote Sensing*, **65**, 2-16. http://dx.doi.org/10.1016/j.isprsjprs.2009.06.004

[18] ALOS/PALSAR Mosaic Product Format (2008) http://www.eorc.jaxa.jp/ALOS/en/kc_mosaic/kc_mosaic.htm

[19] Loew, A. and Mauser, W. (2007) Generation of Geometrically and Radiometrically Terrain Corrected SAR Image Products. *Remote Sensing of Environment*, **106**, 337-349. http://dx.doi.org/10.1016/j.rse.2006.09.002

[20] Shimada, M., Itoh, T., Motooka, T., Watanabe, M., Shiraishi, T., Thapa, R. and Lucas, R. (2014) New Global Forest/ Non-Forest Maps from ALOS PALSAR Data (2007-2010). *Remote Sensing of Environment*, In Press. http://dx.doi.org/10.1016/j.rse.2014.04.014

[21] Akatsuka, S., Takeuchi, W., Rakwatin, P. and Sawada, H. (2009) Evaluation of Slope Correction Effects on ALOS PALSAR Mosaic Data Set in Forest Mappingin Indonesia and Malaysia. 30*th Asian Conference on Remote Sensing*, Beijing, 19-23 October 2009, TS11-03.

[22] Japan Aerospace Exploration Agency (2009) SAR Image Processing Using GRASS in GIS-Knoppix Ver. 1.2. http://www.safe.iis.u-tokyo.ac.jp/pdf/SAR_image_processing_ver1.1.pdf

[23] Kellndorfer, J.M., Pierce, L.E., Dobson, M.C. and Ulaby, F.T. (1998) Toward Consistent Regional-to-Global-Scale Vegetation Characterization Using Orbital SAR Systems. *IEEE Transactions on Geoscience and Remote Sensing*, **36**, 1396-1411. http://dx.doi.org/10.1109/36.718844

[24] Rokhmatuloh, Murfi, H. and Tateishi, R. (2012) Support Vector Machine (SVM) for Classification of Forest and Non Forest Derived from ALOS PALSAR Data. Report and Proceedings of ALOS Application and Verification Project in Indonesia, 18-25.

[25] Castel, T., Beaudoin, A., Stach, N., Stussi, N., Le Toan, T. and Durand, P. (2001) Sensitivity of Space-Borne SAR Data to Forest Parameters over Sloping Terrain. Theory and Experiment. *International Journal of Remote Sensing*, **22**, 2351-2376. http://dx.doi.org/10.1080/01431160121407

[26] Santoro, M., Beer, C., Cartus, O., Schmullius, C., Shvidenko, A., McCallum, I., Wegmuller, U. and Wiesmann, A. (2011) Retrieval of Growing Stock Volume in Boreal Forest Using Hyper-Temporal Series of Envisat ASAR Scan SAR Backscatter Measurements. *Remote Sensing of Environment*, **115**, 490-507. http://dx.doi.org/10.1016/j.rse.2010.09.018

[27] Wegmuller, U. (1999) Automated Terrain Corrected SAR Geocoding. *IEEE Geoscience and Remote Sensing Symposium*, Hamburg, 28 June -2 July 1999, 1712-1714.

[28] Ulander, L.M.H. (1996) Radiometric Slope Correction of Synthetic-Aperture Radar Images. *IEEE Transactions on Geoscience and Remote Sensing*, **34**, 1115-1122. http://dx.doi.org/10.1109/36.536527

[29] Ulaby, F.T., Moore, R.K. and Fung, A.K. (1982) Microwave Remote Sensing, Active and Passive. Artech House, Norwood.

[30] Sun, G., Ranson, K.J. and Kharuk, V.I. (2002) Radiometric Slope Correction for Forest Biomass Estimation from SAR Data in the Western Sayani Mountains, Siberia. *Remote Sensing of Environment*, **79**, 279-287. http://dx.doi.org/10.1016/S0034-4257(01)00279-6

Scientific Research Publishing (SCIRP) is one of the largest Open Access journal publishers. It is currently publishing more than 200 open access, online, peer-reviewed journals covering a wide range of academic disciplines. SCIRP serves the worldwide academic communities and contributes to the progress and application of science with its publication.

Other selected journals from SCIRP are listed as below. Submit your manuscript to us via either submit@scirp.org or Online Submission Portal.